tvst

https://doi.org/10.1167/tvst.8.5.22

Article

# Imaging Distal Aqueous Outflow Pathways in a Spontaneous Model of Congenital Glaucoma

Kevin C. Snyder[1], Kazuya Oikawa[1,2], Jeremy Williams[2], Julie A. Kiland[2], Shaile Gehrke[1], Leandro B. C. Teixeira[3], Alex S. Huang[4], and Gillian J. McLellan[1,2]

[1] Department of Surgical Sciences, School of Veterinary Medicine, University of Wisconsin-Madison, WI, USA
[2] Department of Ophthalmology and Visual Sciences, School of Medicine and Public Health, University of Wisconsin-Madison, WI, USA
[3] Department of Pathobiological Sciences, School of Veterinary Medicine, University of Wisconsin-Madison, WI, USA
[4] Doheny Eye Institute, and Department of Ophthalmology University of California, Los Angeles, CA, USA

**Correspondence:** Gillian J. McLellan, 1300 University Ave, 598 Medical Sciences Center, Madison, WI 53706, USA. e-mail: gillian.mclellan@wisc.edu

**Received:** 2 May 2019
**Accepted:** 26 July 2019
**Published:** 9 October 2019

**Keywords:** aqueous angiography; glaucoma anterior segment; optical coherence tomography; imaging

**Citation:** Snyder KC, Oikawa K, Williams J, Kiland JA, Gehrke S, Teixeira LBC, Huang AS, McLellan GJ. Imaging distal aqueous outflow pathways in a spontaneous model of congenital glaucoma. Trans Vis Sci Tech. 2019;8(5):22, https://doi.org/10.1167/tvst.8.5.22


**Purpose:** To validate the use of aqueous angiography (AA) in characterizing distal aqueous outflow pathways in normal and glaucomatous cats.

**Methods:** Ex vivo AA and optical coherence tomography (OCT) were performed in nine adult cat eyes (5 feline congenital glaucoma [FCG] and 4 normal), following intracameral infusion of 2.5% fluorescein and/or 0.4% indocyanine green (ICG) at physiologic intraocular pressure (IOP). Scleral OCT line scans were acquired in areas of high- and low-angiographic signal. Tissues dissected in regions of high- and low-AA signal, were sectioned and hematoxylin and eosin (H&E)-stained or immunolabeled (IF) for vascular endothelial and perivascular cell markers. Outflow vessel numbers and locations were compared between groups by Student's *t*-test.

**Results:** AA yielded circumferential, high-quality images of distal aqueous outflow pathways in normal and FCG eyes. No AA signal or scleral lumens were appreciated in one buphthalmic FCG eye, though collapsed vascular profiles were identified on IF. The remaining eight of nine eyes all showed segmental AA signal, distinguished by differences in time of signal onset. AA signal always corresponded with lumens seen on OCT. Numbers of intrascleral vessels were not significantly different between groups, but scleral vessels were significantly more posteriorly located relative to the limbus in FCG.

**Conclusions:** A capacity for distal aqueous humor outflow was confirmed by AA in FCG eyes ex vivo but with significant posterior displacement of intrascleral vessels relative to the limbus in FCG compared with normal eyes.

**Translational Relevance:** This report provides histopathologic correlates of advanced diagnostic imaging findings in a spontaneous model of congenital glaucoma.

## Introduction

Primary congenital glaucoma (PCG) is an important cause of blindness in children world-wide.[1,2] Our lab has established and characterized a unique, spontaneous, recessively inherited feline model of PCG with mutation in *LTBP2*,[3,4] which encodes latent transforming growth factor-β binding protein 2, and is a known gene implicated in human PCG (Online Mendelian Inheritance in Man #613086).[5,6] Although LTBP2 plays an important role in the assembly of fibrillin microfibrils in elastic and other tissues, the pathophysiology of glaucoma in humans and cats with *LTBP2* mutation is incompletely understood.[5,7–12] Although it has been suggested that affected cats may have a paucity of scleral vessels,[4] prior studies in the feline model have been limited to small segments of the outflow pathway examined in histologic sections. As this pathway is circumferential, it is critically important to evaluate the outflow structures throughout the full 360° as defects may be localized and segmental.[13,14]

Maintenance of a physiologically normal intraocular pressure (IOP) requires a balance between

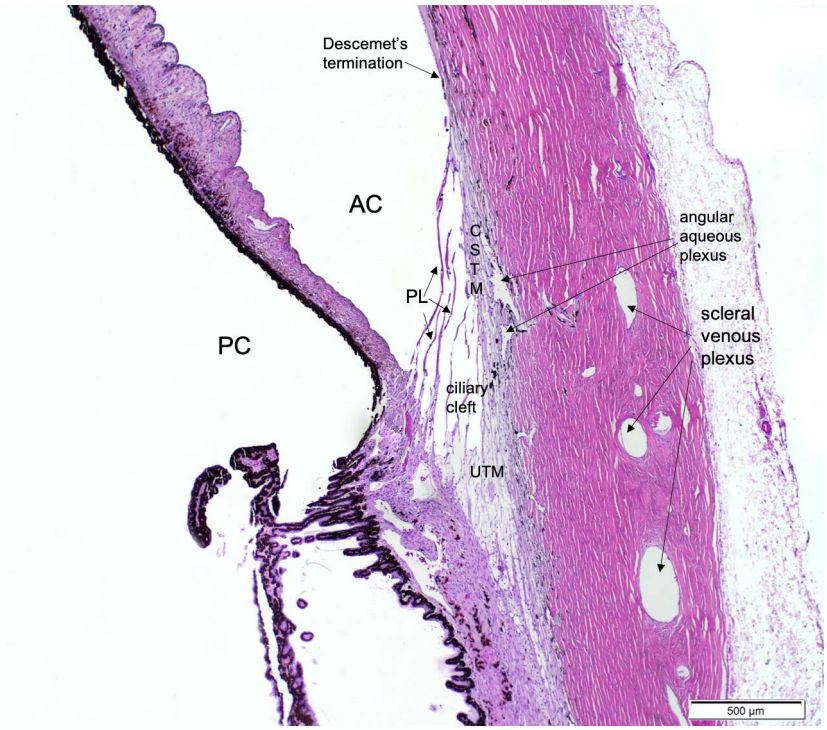


**Figure 1.** Photomicrograph of a normal adult feline iridocorneal angle stained with H&E, illustrating important structures of the feline conventional aqueous outflow pathway. Anterior chamber (AC), posterior chamber (PC), pectinate ligaments (PL), corneoscleral trabecular meshwork (CSTM), Descemet's membrane termination, ciliary cleft, uveoscleral trabecular meshwork (UTM), angular aqueous plexus, and scleral venous plexus are labeled for reference.

aqueous humor production and outflow from the anterior chamber, predominantly via the conventional aqueous outflow pathways.[15–17] Aqueous humor exits the anterior chamber through the trabecular meshwork and Schlemm's canal proximally, then outflow continues distally via collector channels and, in humans, a small caliber intrascleral venous plexus, and via aqueous veins to the episcleral veins. Despite interspecies differences in aqueous humor outflow pathway morphology, principally in the lack of a circumferential Schlemm's canal in dogs and cats,[18–20] underlying physiology is broadly comparable, as the inner wall of the canine and feline angular aqueous plexus is similar in function to the inner "vacuolating endothelium" of Schlemm's canal[20] (Fig. 1). The morphology of the conventional aqueous outflow pathways, including the trabecular meshwork, juxtacanalicular tissue, angular aqueous plexus, collector channels, and intrascleral venous plexus has not yet been comprehensively characterized in cats with feline congenital glaucoma (FCG).[4]

A unifying feature of PCG, identified in limited histologic studies of affected human eyes, is the apparent arrest in "canalization" of these modified vascular channels responsible for conventional aqueous humor outflow from the anterior chamber.[21–26] Similarly, preliminary light microscopic studies in this FCG *LTBP2* model identified structural abnormalities in the outflow pathways suggestive of developmental arrest of these pathways.[4] Although the clinical course of disease in affected animals has been well-characterized, underlying pathology of the aqueous outflow pathways that contributes to elevated IOP has not yet been fully delineated in this model.

With the advent of increasingly advanced imaging technology, there have been numerous studies in the past 10 years imaging various components of the eye and outflow pathways, including spectral-domain optical coherence tomography (SD-OCT) three-dimensional (3D) reconstruction in ex vivo[27–29] and in vivo[30] human eyes, optical clearing methods in ex vivo mouse[31] and pig eyes,[32] and re-perfusion canalograms and fluorescent microspheres in ex vivo pig[33,34] and human[35] eyes. Dynamic aqueous outflow imaging in pig,[36] bovine,[37] monkey,[38] and human[36,39] eyes by aqueous angiography (AA) improve on existing techniques by providing real-time information on circumferential, posttrabecular components of the conventional aqueous outflow pathways, including in vivo under physiologic conditions in human eyes.[39]

We hypothesize that distal aqueous outflow pathway morphology is abnormal in cats homozygous for *LTBP2* mutation. Our aim was to apply the technique of AA to our feline model of spontaneous congenital glaucoma to facilitate circumferential characterization of the distal aqueous outflow pathways in normal and glaucomatous cats. To our knowledge, this is the first report of AA in a spontaneous model of congenital glaucoma.

# Methods

## Aqueous Angiography

Eyes from five cats with FCG and four normal feline eyes, all from young adult cats (age range 1–4 years), were studied. Eyes were obtained postmortem with adnexa intact from animals euthanized for reasons unrelated to this specific study, in compliance with Institutional Animal Care and Use Committee protocols and the ARVO statement for the Use of Animals in Ophthalmic and Vision Research. AA was performed in eyes ex vivo within 4 hours postmortem as previously described for pig, bovine, and human eyes.[36,37] Prior to imaging, eyes were kept moist in a sealed container with phosphate-buffered saline (PBS)-soaked gauze at 4°C. Orientation of superior, inferior, nasal, and temporal quadrants in each globe was verified based on the direction of the attached optic nerve, position of long posterior ciliary arteries, inferior oblique muscle insertion, and position of the nictitating membrane prior to pinning the globe to soft modeling clay. A 20-G Lewicky anterior chamber maintainer (Accutome, Malvern, PA) was inserted into the anterior chamber through a 22-G side-port incision in the limbal cornea and connected to a fluid reservoir containing balanced salt solution (BSS; Alcon, Fort Worth, TX). The location of the anterior chamber maintainer was assigned to either the 3 or 9 o'clock position for each eye. The height of the BSS reservoir was adjusted as necessary to maintain IOP at 12 to 18 mm Hg for 30 minutes (i.e., within the IOP reference range established for normal felines[40]), as confirmed by rebound tonometry using the Icare TONOVET (Icare, Vantaa, Finland).[41] The cornea was kept moist with BSS drops administered topically every 3 to 5 minutes. Following the 30-minute preperfusion period, 0.4% indocyanine green (ICG) in BSS was introduced into the anterior chamber at physiologic IOP, followed sequentially by 2.5% fluorescein (Akorn, Decatur, IL) diluted in BSS in five of nine eyes. These concentrations and subsequent order were selected on the basis of previously published reports of AA in enucleated pig and human eyes.[36] The final four eyes tested received only 0.4% ICG due to its similar angiographic pattern to fluorescein but longer intraluminal presence. Briefly, immediately prior to imaging, aqueous humor was exchanged for the respective dye solution, which was allowed to flow into the eye under gravity at physiologic IOP. The reservoir height of the tracer was adjusted as needed to maintain physiologic IOP within the prespecified physiologic range.[36]

AA was performed using the Spectralis HRA-OCT (Heidelberg Engineering, Inc., Heidelberg, Germany) with an anterior-segment module lens. Immediately before tracer introduction, confocal scanning laser ophthalmoscope (cSLO) infrared images were obtained to center the eye and optimize image focus. Fluorescent angiography images were taken to document background fluorescence intensity of the tissues. Image acquisition of angiographic signal commenced immediately upon tracer infusion, and images were acquired for up to 20-minutes posttracer infusion, or up to timepoints at which the angiographic signal was over saturated, precluding visualization of small vessel anatomy. Though the sensitivity was initially set at 50 for each eye, it was then adjusted as necessary to prevent image oversaturation and provide optimal fine detail in angiographic images for as long after tracer introduction as possible. Images were acquired from each perilimbal quadrant, at time intervals of 3 to 4 minutes. For purposes of comparison, "high-AA signal" regions were defined as those with any signal immediately present within the first 10 minutes, and "low-AA signal" regions had no initial angiographic signal, developing signal between 15 and 20 minutes after tracer introduction.

## Spectral-Domain Optical Coherence Tomography (SD-OCT)

Concurrently, scleral line scans were obtained using Spectralis HRA+OCT with the anterior-segment module, in Sclera mode. Single line scans were acquired with a 15° scan angle. Images were acquired to determine whether angiographic signal corresponded with hyporeflective signal voids consistent with lumens on OCT, and to enable comparison of morphologic features between regions of high- and low-AA signal. Scleral line scans were acquired in an orientation that was approximately perpendicular to the limbus.

## OCT and AA Image Analyses

OCT and AA images were analyzed using Heidelberg Spectralis software, Heidelberg Eye Explorer (HEYEX, 2014) and ImageJ BioFormats v5.8 Plugin (http://imagej.nih.gov/ij/; provided in the public domain by the National Institutes of Health, Bethesda, MD, USA).

Images were reviewed, and three high-resolution OCT and AA image pairs from high- and low-AA signal quadrants, showing AA signal architecture, were selected and analyzed from each eye. Number of scleral lumens identified in OCT scans were statistically compared using two-tailed unpaired Student's *t*-test between disease and control groups as well as between high- and low-AA signal regions.

## Immunofluorescent Labeling

Eyes were perfusion fixed within a physiologic range of feline IOP (12–18 mm Hg) with 4% paraformaldehyde in 0.1 M PBS (PFA) for 10 minutes at room temperature, then immersed overnight in 4% PFA at 4°C before transfer to 0.1 M PBS. The anterior segment of each globe was removed by circum-equatorial incision and dissected into two radial sectors per high- and low-signal quadrant, as previously identified by AA. Tissue samples from each quadrant of the anterior segment of each eye were cryoprotected by immersion in 15% sucrose in 1× PBS until the tissue sank, then transferred to 30% sucrose in 1× PBS. The tissue samples were then embedded and cryosectioned at 10 µm and slides stored at −80°C prior to immunolabeling (IF). After permeabilization and blocking in a solution of 10% normal donkey serum (NDS), 1% bovine serum albumin (BSA) and 0.1% Triton-X100 in 0.01 M PBS, for 1 hour at room temperature, cryosections were incubated overnight in 2% NDS, 1% BSA, and 0.05% Tween-20 in 0.01 M PBS at 4°C with primary antibodies that label perivascular cells (alpha-SMA, at 1:400 dilution in 0.01 M PBS; Novus Biologicals, Centennial, CO) and a vascular endothelial marker (von Willebrand Factor [vWF], at 1:2000 dilution in 0.01 M PBS; Novus Biologicals). Primary antibodies were detected by appropriate Alexa Fluor 568 and 647 conjugated secondary antibodies at 1:400 dilution in 0.01 M PBS and nuclei counterstained with DAPI (1:10000 dilution in 0.01 M PBS) in 1% BSA and 0.05% Tween-20 in 0.01 M PBS. Cryosections of feline tissue (liver, spleen, or kidney) served as positive controls, and negative controls for each run omitted the primary antibody replacing it with nonimmune serum from the same species. After washing and mounting in antifade aqueous mounting medium (ProLong Gold; Invitrogen, Carlsbad, CA), each slide was examined and photomicrographs for subsequent image analysis were obtained at ×20 magnification (Axio Imager fluorescence microscope with Zen Pro software v2.3; Zeiss, Oberkochen, Germany).

## Distal Outflow Pathway Histomorphometric Analysis

Histopathology of the same nine eyes allowed further morphologic characterization of the distal outflow pathways. Photomicrographs of the distal outflow pathway were analyzed from three IF cryosections, obtained from a high-AA signal region and three sections from a low AA signal region for each eye, by a masked observer using ImageJ BioFormats v5.8 Plugin. Scleral vessels were counted if there was a scleral lumen posterior to the termination of Descemet's membrane that was highlighted by both IF markers, vWF and alpha-SMA.

Additionally, scleral lumen circumference and cross-sectional area of the scleral vessels were measured. Preliminary descriptive statistics showed a bimodal distribution of scleral vessel lumen size in normal cats, with clear delineation between 95% confidence intervals for the two distinct "populations" of scleral lumens, that was readily appreciable on qualitative evaluation of photomicrographs. Thus, vessels 500 µm or more in circumference were classified as "large" and vessels less than 500 µm were classified as "small" for the purposes of subsequent analyses. Circumference was selected as a quantitative measure of vessel size because in one FCG eye, scleral vessel lumens were collapsed, precluding meaningful measurement of area. Distance in micrometers was measured from the termination of Descemet's membrane both to the first small vessel lumen and to the first large vessel lumen in each section (Supplemental Fig. S1). Parameters were compared between control and glaucoma groups, and between high- and low-AA signal regions regardless of phenotype, by two-tailed unpaired Student's *t*-test (Prism 8.1.0; GraphPad Software, San Diego, CA). A $P$ value $\leq 0.05$ was considered statistically significant.

# Results

## Aqueous Angiography and SD-OCT

AA yielded circumferential, high-quality images of distal aqueous outflow pathways in both normal and

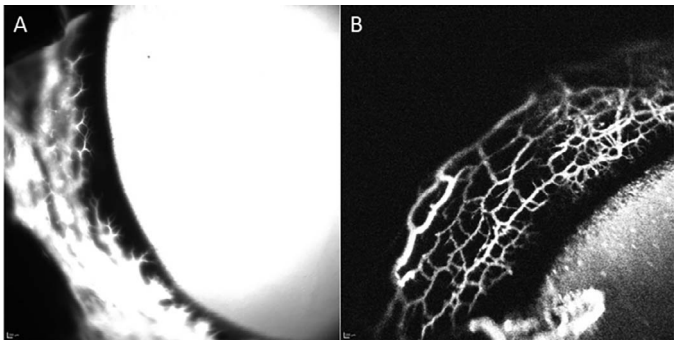


**Figure 2.** ICG (0.4%) yielded higher resolution images for longer imaging time versus 2.5% fluorescein as a tracer. (A) Representative image of angiographic signal in a normal feline eye with 2.5% fluorescein 10 minutes after intracameral infusion. Note the diffuse loss of detail and lack of outflow architecture due to fluorescein diffusion. (B) Representative image of angiographic signal in a normal feline eye with 0.4% ICG approximately 12 minutes after injection. Note improved resolution and detail of outflow architecture.

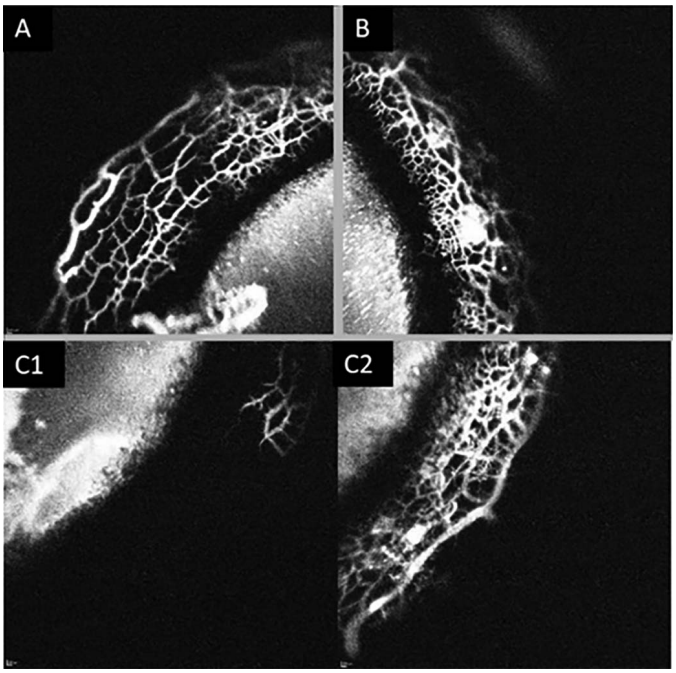


**Figure 3.** Segmental outflow in a normal feline eye. Images of three quadrants (A–C) from the same eye taken at approximately 7 minutes post 0.4% ICG injection. (A, B) Depict high-angiographic signal and (C1) depicts no signal. (C2) depicts the same quadrant as in (C1), imaged at 20 minutes postinjection of tracer, which now exhibits an angiographic signal.

FCG eyes. Initially, both 2.5% fluorescein and 0.4% ICG were used in five eyes (3 affected, 2 normal) before switching to only testing with ICG in the remaining eyes. Use of ICG as a tracer yielded more defined vascular images compared with fluorescein for longer, but with no overall qualitative differences in outflow architecture (Fig. 2).

Segmental regions of AA signal, distinguished by differences in time of signal onset but not by qualitative differences in the ultimate signal intensity, were observed in eight of nine eyes (Fig. 3). No AA vascular appearing signal was appreciated in one severely affected buphthalmic FCG eye. Instead, there appeared a diffuse signal pattern that did not mirror typical aqueous and episcleral veins and no hyporeflective, intrascleral lumens were observed with OCT (Fig. 4).

In the remaining eight of nine eyes, the observed AA signal appeared vascular in nature and corresponded with scleral lumens that were appreciated on OCT. Simultaneous SD-OCT images obtained in areas of high-angiographic signal confirmed that angiographic signal corresponded with scleral lumens. The perilimbal regions that showed the fastest developing AA signal were not distributed in a consistent quadrant, but the inferior-temporal quadrant was most frequently the low-signal quadrant, as identified in six of eight eyes. For all eyes that displayed segmental outflow, the areas of low angiographic signal still displayed open scleral lumens on OCT (Fig. 5). These low-angiographic signal areas ultimately developed AA signal after an extended imaging time, ranging from 15 to 20 minutes posttracer infusion and were recognized and comparable in animals from both normal and FCG groups (Fig. 3).

Mean number of intrascleral vessels observed on OCT was not significantly different between normal and FCG groups ($P = 0.07$) despite a trend toward FCG cats having fewer intrascleral vessels. Mean number of intrascleral vessels on OCT was also not significantly different between high- and low-signal regions, irrespective of glaucoma status ($P = 0.52$). As represented in Figure 4, collector channels and intrascleral vessels appeared posteriorly displaced, relative to the limbus in eyes with FCG compared with controls. Quantitative analysis of this observed relationship was not attempted in OCT images due to lack of consistent landmarks and exact line scan orientation.

## Histomorphometry

On hematoxylin and eosin (H&E)-stained sections, normal feline eyes had easily identifiable scleral lumens, consistent in number and appearance with those observed on OCT. However, in glaucoma eyes, and particularly the most severely affected eye, it was

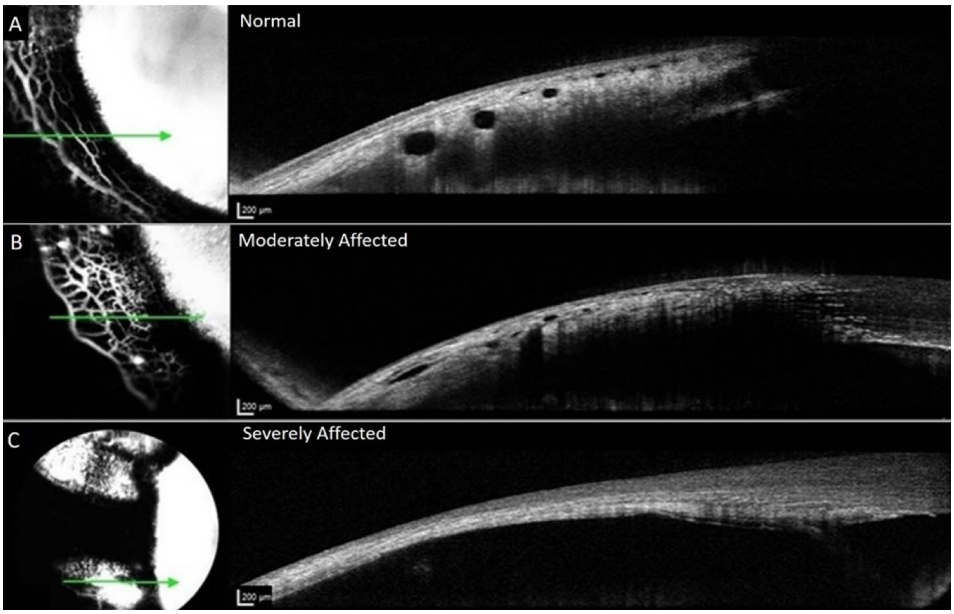


**Figure 4.** Representative OCT images from normal and glaucomatous feline eyes. Images on the *left* represent en face confocal laser scanning ophthalmoscopy images of AA signal and images on the right are corresponding, OCT line scans registered to these images **Green arrow* corresponds to precise location of OCT line scan. (A) Depicts normal eye; (B) depicts globe affected by glaucoma. OCT lumens visible but appear attenuated. (C) Depicts severely affected glaucoma eye with no vascular outflow signal, or scleral lumens visible on the corresponding OCT image. The sclera is thin and no scleral vessel lumens are visible. Angiographic signal on the left represents combination of diffusion into overlying conjunctival tissues after extended period of time and possibly signal visible from within, through extremely thin sclera.

difficult to distinguish attenuated or collapsed scleral lumens from artifacts of histologic sectioning. Overall, histopathologic findings and IF corroborated the OCT observations in ex vivo eye preparations (Fig. 6). The termination of Descemet's membrane was used as a consistent anatomic landmark, and only scleral lumens posterior to this point were included in our analysis (Fig. 7).

Significant differences were observed when comparing distance from the termination of Descemet's membrane to the first small and large vessel lumens between normal and glaucoma groups ($P = 0.001$ and $P \leq 0.0001$, respectively). Both large and small scleral vessels were significantly more posterior in location in eyes with glaucoma than in normal eyes (Fig. 8). A statistically significant difference in this distance was not seen when comparing high- and low-signal regions in cats from both groups (Fig. 9).

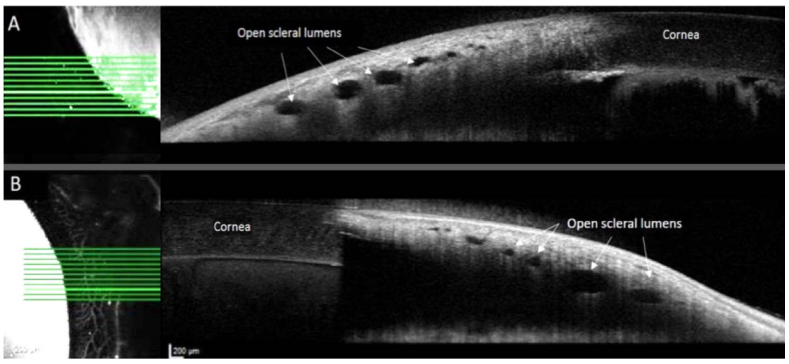


**Figure 5.** Open scleral lumens were observed on OCT images (*right*), both in regions of low-AA signal (A), and of high-AA signal (B) in different quadrants of the same representative normal feline eye taken consecutively at approximately 9 minutes postinjection of 0.4% iCG. Brightest horizontal lines on en face AA images (*left*) correspond to location of respective OCT line scans on *right*.

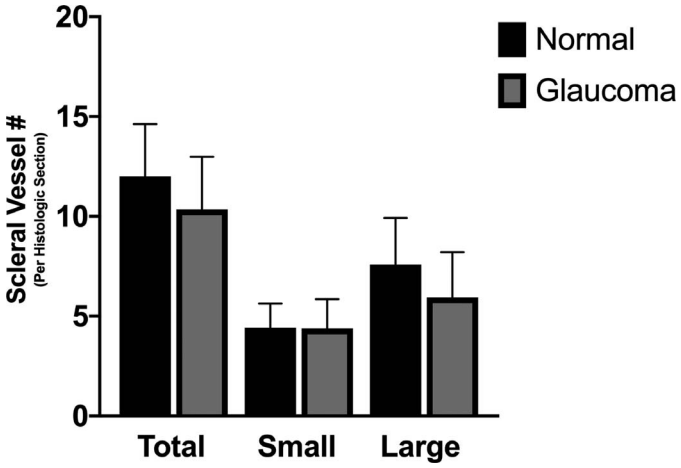


**Figure 6.** Number of scleral vessels identified on IF histologic sections did not differ between normal cats and cats with feline congenital glaucoma. Total number of scleral vessels, number of large scleral vessels (>500 μm in circumference), and number of small scleral vessels (<500 μm in circumference) were not significantly different between glaucoma affected and normal eyes. *Error bars* represent standard deviation.

Collapsed scleral lumens, that were not identified by AA or scleral OCT, were identified by IF in the most severely affected eye. The angular aqueous plexus (AAP) was only consistently identifiable in normal cat tissue sections and was not consistently observed in all of the FCG-affected sections. AAP present in normal cat sections labeled positively for vWF, but not with alpha-SMA antibody, consistent with previous reports.[42,43] In select cases, the AAP could be visualized in close association with collector channels (Fig. 10).

## Discussion

To our knowledge, this is the first report of AA conducted in spontaneous congenital glaucoma in any species. The use of 0.4% ICG yielded high-quality images of the distal, posttrabecular aqueous humor outflow pathways in all but the most severely affected eye ex vivo. The reported experiments provide proof of concept and validate the use of the AA technique in glaucoma models ex vivo.

AA images, consistent with previous reports, suggested a segmental nature of aqueous humor outflow, both in this feline model of congenital glaucoma as well as normal feline eyes. Segmental aqueous humor outflow has been identified previously by different methods in mouse, bovine, monkey, and human eyes.[44–51]

The OCT images acquired simultaneously with AA

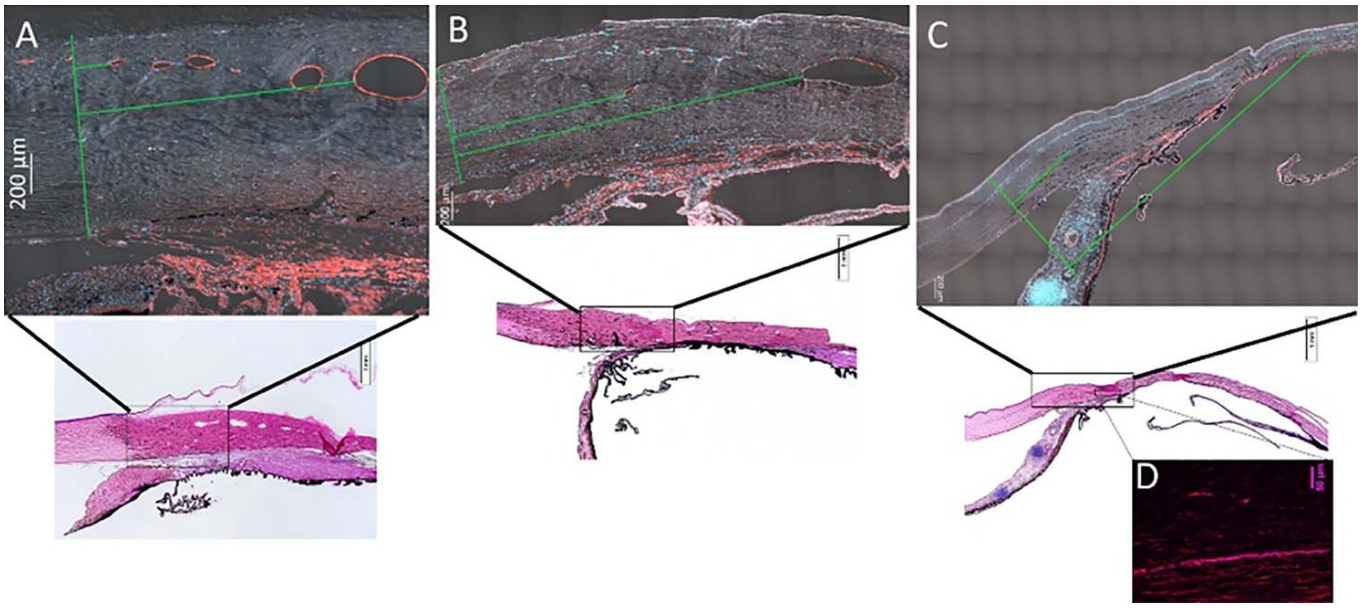


**Figure 7.** Representative, tiled sections from feline anterior segment tissues IF labeled for vascular endothelial cells with vWF (*red*) and DAPI nuclear counterstain (*blue*) include differential interference contrast (DIC) signal for visualization of scleral tissue (A–C). (A) Normal eye, (B) moderately affected eye, and (C, D) severely affected eye, in which collapsed scleral vessel lumens were observed with IF (D) that were not visible on OCT. **Green line* on *left* of each image is a line drawn perpendicularly to sclera corresponding to the termination of Descemet's membrane and *two perpendicular green lines* depict distance measured to first small scleral vessel lumen and first large vessel lumen.

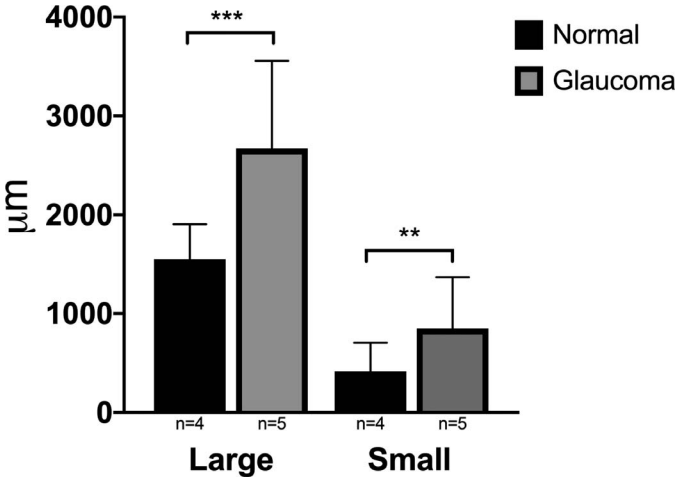


Figure 8. Mean distance in micrometers from the termination of Descemet's membrane to first large and small vessel lumen, comparing normal and glaucoma groups from histologic sections. These distances were significantly greater in eyes with glaucoma than in normal eyes ($P \leq 0.0001$ and $P = 0.001$, respectively). *Error bars* represent standard deviation.

in regions of high- and low-AA signal allowed within-eye comparisons of the lumen number and architecture. The lack of differences in scleral lumens appreciated on OCT analyses between these different "signal" regions could be attributable to segmental differences in more proximal, trabecular meshwork biology, or energy-dependent mechanisms regulating aqueous outflow, that are not amenable to study in our preparations ex vivo. Previous analysis using OCT in humans to examine Schlemm's canal and

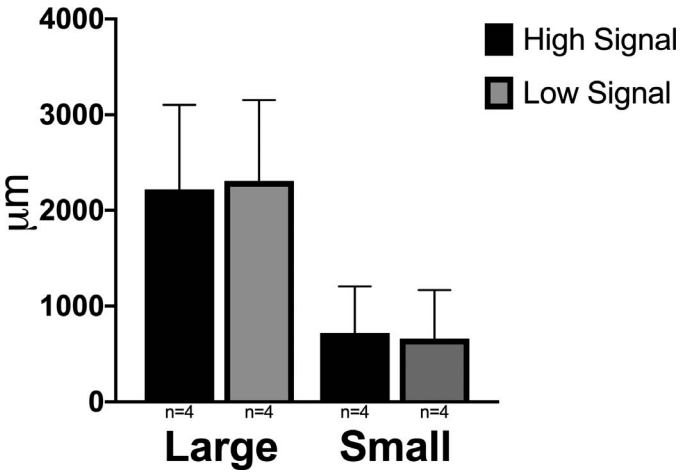


Figure 9. Mean distances in micrometers from the termination of Descemet's membrane to either the first large or first small vessel lumen were not significantly different between histologic sections from high AA signal and low AA signal regions. *Error bars* represent standard deviation.

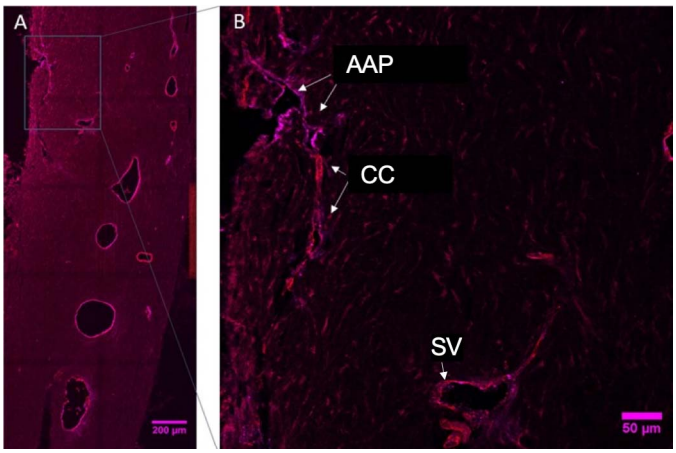


Figure 10. (A) Immunofluorescent labelled section through the perilimbal region of a representative normal feline eye (image is intentionally overexposed to allow visualization of tissue morphology) with region delineated by a *rectangle* shown at higher magnification in (B), which depicts the location of the normal AAP labeled positively with vWF (endothelial cells; *magenta*) while the collector channels (CC) and scleral vessels (SV) are positively labeled for both vWF and alpha-smooth muscle actin (perivascular cells; *red*).

associated collector channels and scleral venous plexus identified reduced Schlemm's canal cross-sectional area in a small number of in vivo human glaucoma eyes with IOP elevation.[52] In ex vivo pig eyes, 3D reconstruction of the outflow pathway following optical clearing and confocal microscopy identified segmental variations in collector channel size.[32] Our combined AA and OCT images provided valuable circumferential structural information in the distal outflow pathway of the feline eye, but did not afford sufficient resolution of the circumferential, small diameter, branching AAP to substantially illuminate structure and physiology of more proximal components of the conventional aqueous outflow pathway in this model. Further experiments to evaluate morphology of the trabecular meshwork, juxtacanicular tissue, and AAP at an ultrastructural level will be critical to better understanding the nature of segmental aqueous outflow and its potential physiologic significance in FCG.

The cause of apparent displacement of scleral lumens observed between normal and glaucoma groups may be multifactorial. As this study was conducted in adult cats, the cats with FCG had been exposed to fluctuating IOP between 30 and 40 mm Hg throughout their lifetimes, with intermittent spikes in IOP to 50 to 70 mm Hg, with the most severely affected cat displaying consistently elevated IOP near

end-stage disease, and with grossly apparent buphthalmos in one eye. Although the other four of five eyes were not appreciably buphthalmic on clinical examination, it is conceivable that stretching of the sclera may have disrupted normal anatomic proportions and relationships in the distal aqueous outflow pathway, in turn contributing to increased distance observed from termination of Descemet's membrane to scleral vascular plexus. Alternatively, relative posterior location of the scleral lumens could represent underlying developmental differences in the maturation of the distal aqueous outflow pathway in affected cats. Posterior displacement of the lumens could lead to greater distal resistance to aqueous outflow predisposing the eye to increased IOP. While the juxtacanicular tissue of the trabecular meshwork is widely accepted as a major source of aqueous outflow resistance in human glaucoma,[53–56] distal outflow resistance has also been shown in multiple studies to contribute to resistance to aqueous outflow.[56–63] However, the present study was not designed to determine cause and effect relationships. Further studies will be necessary in FCG eyes prior to onset of significant elevation in IOP,[58] to determine whether morphologic differences in the distal outflow pathway are primarily developmental or represent a secondary effect of buphthalmos.[64]

The identification of collapsed scleral lumens using IF in the most severely affected eye confirmed the presence of scleral lumens in the distal outflow pathway that were not identifiable on conventional histopathology or by anterior-segment OCT. Thus, in both research and clinical settings, a lack of scleral lumens observed on OCT images, or even routine ocular histopathology, does not necessarily equate to true absence of scleral lumens. Rather, our findings illustrate that scleral lumens could be present but may be collapsed, with no visible luminal area.

Importantly, for most cases, in the absence of gross globe stretching and gross enlargement, when IOP is normalized, OCT does identify lumens associated with the distal outflow pathway and our IF labeling corroborated both AA and OCT findings. This has important implications for clinicians using OCT to examine the anterior segment in adult and pediatric glaucoma patients, as OCT is able to noninvasively identify components of the distal outflow pathway but may be unable to detect the presence of collapsed lumens. Conclusions made from analysis of OCT images should always consider this important possibility, particularly as it may prove difficult to image eyes at normal IOP in a clinical setting.

Limitations of the current study, that are often inherent in studies involving "large" animal models, include the small number of eyes used. As this was designed as a pilot study, the small sample size is considered adequate to provide proof-of-concept for AA and histopathology. Morphologic relationships appreciated on histopathology will need to be evaluated in studies with a larger sample size. Our histopathology and IF analyses were limited to cross sections taken of an extensive circumferentially oriented outflow pathway. Potential impact of oblique sectioning for OCT and histomorphometry also should be considered when interpreting our results. Additionally, cell death must be considered in the use of postmortem eyes. However, eyes were used very soon after death (within 4 hours). Previous publications using AA in postmortem human eyes[36,65] showed similar results to eyes from living human subjects.[39,66,67] AA in feline eyes in vivo can also be performed in the future to address these concerns as well.

In conclusion, AA is a valid technique to image aqueous outflow pathways in our spontaneous model of feline glaucoma. Simultaneous OCT imaging can identify scleral lumens noninvasively in all but the most severely affected globes, but caution should be exercised when interpreting OCT results, as we also demonstrated that collapsed or compressed lumens may be present, but not perfused or visible on OCT. While aqueous outflow appears to exhibit segmental behavior in cats, this cannot be readily explained by morphologic differences in the distal outflow pathway in this ex vivo model and may reflect segmental trabecular meshwork biology. The distal outflow pathway is posteriorly displaced relative to the limbus in this model of congenital glaucoma, when compared with normal subjects, although whether this represents cause or effect of IOP elevation remains to be established.

## Acknowledgments

Supported by National Institutes of Health Grants P30 EY016665, S10 OD018221 (GJM), and K08EY0246474 (ASH); Grants from the Lions Eye Bank of Wisconsin and The Marfan Foundation (GJM); Research to Prevent Blindness Career Development Award (ASH) and unrestricted funds to the Department of Ophthalmology and Visual Sciences, UW-Madison from Research to Prevent Blindness.

Disclosure: **K.C. Snyder**, None; **K. Oikawa**, None; **J. Williams**, None; **J.A. Kiland**, None; **S. Gehrke**, None; **L.B.C. Teixeira**, None; **A.S. Huang**, Heidelberg Engineering, Glaukos Corporation, Diagnosys (F), Aerie Pharmaceuticals (C); **G.J. McLellan**, Icare Finland Oy (F), OcuScience (R)

## References


1. Thylefors B, Négrel AD. The global impact of glaucoma. *Bull World Health Organ*. 1994;72:323–326.
2. Steinkuller PG, Du L, Gilbert C, Foster A, Collins ML, Coats DK. Childhood blindness. *J AAPOS*. 1999;3:26–32.
3. Rutz-Mendicino MM, Snella EM, Jens JK, et al. Removal of potentially confounding phenotypes from a Siamese-derived feline glaucoma breeding colony. *Comp Med*. 2011;61:251–257.
4. Kuehn MH, Lipsett KA, Menotti-Raymond M, et al. A mutation in LTBP2 causes congenital glaucoma in domestic cats (*Felis catus*). *PLoS One*. 2016;11:e0154412.
5. Ali M, McKibbin M, Booth A, et al. Null mutations in LTBP2 cause primary congenital glaucoma. *Am J Hum Genet*. 2009;84:664–671.
6. Narooie-Nejad M, Paylakhi SH, Shojaee S, et al. Loss of function mutations in the gene encoding latent transforming growth factor beta binding protein 2, LTBP2, cause primary congenital glaucoma. *Hum Mol Genet*. 2009;18:3969–3977.
7. Hirai M, Horiguchi M, Ohbayashi T, Kita T, Chien KR, Nakamura T. Latent TGF-beta-binding protein 2 binds to DANCE/fibulin-5 and regulates elastic fiber assembly. *EMBO J*. 2007;26:3283–3295.
8. Inoue T, Ohbayashi T, Fujikawa Y, et al. Latent TGF-β binding protein-2 is essential for the development of ciliary zonule microfibrils. *Hum Mol Genet*. 2014;23:5672–5682.
9. De Maria A, Wilmarth PA, David LL, Bassnett S. Proteomic analysis of the bovine and human ciliary zonule. *Invest Ophthalmol Vis Sci*. 2017;58:573–585.
10. Maumenee AE. The pathogenesis of congenital glaucoma: a new theory. *Trans Am Ophthalmol Soc*. 1958;56:507–570.
11. Broughton WL, Fine BS, Zimmerman LE. Congenital glaucoma associated with a chromosomal defect. A histologic study. *Arch Ophthalmol*. 1981;99:481–486.
12. Hollander DA, Sarfarazi M, Stoilov I, Wood IS, Fredrick DR, Alvarado JA. Genotype and phenotype correlations in congenital glaucoma. *Trans Am Ophthalmol Soc*. 2006;104:183–195.
13. van der Merwe EL, Kidson SH. The three-dimensional organisation of the post-trabecular aqueous outflow pathway and limbal vasculature in the mouse. *Exp Eye Res*. 2014;125:226–235.
14. Kizhatil K, Ryan M, Marchant JK, Henrich S, John SW. Schlemm's canal is a unique vessel with a combination of blood vascular and lymphatic phenotypes that forms by a novel developmental process. *PLoS Biol*. 2014;12:e1001912.
15. Civan MM, Macknight AD. The ins and outs of aqueous humour secretion. *Exp Eye Res*. 2004;78:625–631.
16. Formation Anders B. and drainage of aqueous humour in cats. *Exp Eye Res*. 1966;5:185–190.
17. Carreon T, van der Merwe E, Fellman RL, Johnstone M, Bhattacharya SK. Aqueous outflow - a continuum from trabecular meshwork to episcleral veins. *Prog Retin Eye Res*. 2017;57:108–133.
18. Van Buskirk EM. The canine eye: the vessels of aqueous drainage. *Invest Ophthalmol Vis Sci*. 1979;18:223–230.
19. Tripathi RC, Tripathi BJ. The mechanism of aqueous outflow in lower mammals. *Exp Eye Res*. 1972;14:73–79.
20. Tripathi RC. Ultrastructure of the exit pathway of the aqueous in lower mammals. (A preliminary report on the "angular aqueous plexus"). *Exp Eye Res*. 1971;12:311–314.
21. Maumenee AE. The pathogenesis of congenital glaucoma; a new theory. *Am J Ophthalmol*. 1959;47:827–858.
22. Tawara A, Inomata H. Developmental immaturity of the trabecular meshwork in congenital glaucoma. *Am J Ophthalmol*. 1981;92:508–525.
23. McMenamin PG. A morphological study of the inner surface of the anterior chamber angle in pre and postnatal human eyes. *Curr Eye Res*. 1989;8:727–739.
24. McMenamin PG. Human fetal iridocorneal angle: a light and scanning electron microscopic study. *Br J Ophthalmol*. 1989;73:871–879.
25. Bakunowicz-Lazarczyk A, Sulkowska M, Sulkowski S, Urban B. Ultrastructural changes in the trabecular meshwork of congenital glaucoma. *J Submicrosc Cytol Pathol*. 2001;33:17–22.
26. Hollander DA, Sarfarazi M, Stoilov I, Wood IS, Fredrick DR, Alvarado JA. Genotype and

phenotype correlations in congenital glaucoma: CYP1B1 mutations, goniodysgenesis, and clinical characteristics. *Am J Ophthalmol*. 2006;142:993–1004.
27. Kagemann L, Wollstein G, Ishikawa H, et al. 3D visualization of aqueous humor outflow structures in-situ in humans. *Exp Eye Res*. 2011;93:308–315.
28. Francis AW, Kagemann L, Wollstein G, et al. Morphometric analysis of aqueous humor outflow structures with spectral-domain optical coherence tomography. *Invest Ophthalmol Vis Sci*. 2012;53:5198–5207.
29. Kagemann L, Wollstein G, Ishikawa H, et al. Identification and assessment of Schlemm's canal by spectral-domain optical coherence tomography. *Invest Ophthalmol Vis Sci*. 2010;51:4054–4059.
30. Kagemann L, Wollstein G, Ishikawa H, et al. Visualization of the conventional outflow pathway in the living human eye. *Ophthalmology*. 2012;119:1563–1568.
31. Henning Y, Osadnik C, Malkemper EP. EyeCi: Optical clearing and imaging of immunolabeled mouse eyes using light-sheet fluorescence microscopy. *Exp Eye Res*. 2018;180:137–145.
32. Waxman S, Loewen RT, Dang Y, Watkins SC, Watson AM, Loewen NA. High-resolution, three-dimensional reconstruction of the outflow tract demonstrates segmental differences in cleared eyes. *Invest Ophthalmol Vis Sci*. 2018;59:2371–2380.
33. Loewen RT, Brown EN, Scott G, Parikh H, Schuman JS, Loewen NA. Quantification of focal outflow enhancement using differential canalograms. *Invest Ophthalmol Vis Sci*. 2016;57:2831–2838.
34. Loewen RT, Brown EN, Roy P, Schuman JS, Sigal IA, Loewen NA. Regionally discrete aqueous humor outflow quantification using fluorescein canalograms. *PLoS One*. 2016;11:e0151754.
35. Cha ED, Xu J, Gong L, Gong H. Variations in active outflow along the trabecular outflow pathway. *Exp Eye Res*. 2016;146:354–360.
36. Saraswathy S, Tan JC, Yu F, et al. Aqueous angiography: real-time and physiologic aqueous humor outflow imaging. *PLoS One*. 2016;11:e0147176.
37. Huang AS, Saraswathy S, Dastiridou A, et al. Aqueous angiography with fluorescein and indocyanine green in bovine eyes. *Transl Vis Sci Technol*. 2016;5(6):5.
38. Huang AS, Li M, Yang D, Wang H, Wang N, Weinreb RN. Aqueous angiography in living nonhuman primates shows segmental, pulsatile, and dynamic angiographic aqueous humor outflow. *Ophthalmology*. 2017;124:793–803.
39. Huang AS, Camp A, Xu BY, Penteado RC, Weinreb RN. Aqueous angiography: aqueous humor outflow imaging in live human subjects. *Ophthalmology*. 2017;124:1249–1251.
40. Rusanen E, Florin M, Hässig M, Spiess BM. Evaluation of a rebound tonometer (Tonovet) in clinically normal cat eyes. *Vet Ophthalmol*. 2010;13:31–36.
41. McLellan GJ, Kemmerling JP, Kiland JA. Validation of the TonoVet® rebound tonometer in normal and glaucomatous cats. *Vet Ophthalmol*. 2013;16:111–118.
42. Lei Y, Overby DR, Read AT, Stamer WD, Ethier CR. A new method for selection of angular aqueous plexus cells from porcine eyes: a model for Schlemm's canal endothelium. *Invest Ophthalmol Vis Sci*. 2010;51:5744–5750.
43. Krohn J. Expression of factor VIII-related antigen in human aqueous drainage channels. *Acta Ophthalmol Scand*. 1999;77:9–12.
44. Sabanay I, Gabelt BT, Tian B, Kaufman PL, Geiger B. H-7 effects on the structure and fluid conductance of monkey trabecular meshwork. *Arch Ophthalmol*. 2000;118:955–962.
45. Lu Z, Overby DR, Scott PA, Freddo TF, Gong H. The mechanism of increasing outflow facility by rho-kinase inhibition with Y-27632 in bovine eyes. *Exp Eye Res*. 2008;86:271–281.
46. Battista SA, Lu Z, Hofmann S, Freddo T, Overby DR, Gong H. Reduction of the available area for aqueous humor outflow and increase in meshwork herniations into collector channels following acute IOP elevation in bovine eyes. *Invest Ophthalmol Vis Sci*. 2008;49:5346–5352.
47. Swaminathan SS, Oh DJ, Kang MH, et al. Secreted protein acidic and rich in cysteine (SPARC)-null mice exhibit more uniform outflow. *Invest Ophthalmol Vis Sci*. 2013;54:2035–2047.
48. Hann CR, Bahler CK, Johnson DH. Cationic ferritin and segmental flow through the trabecular meshwork. *Invest Ophthalmol Vis Sci*. 2005;46:1–7.
49. Ethier CR, Chan DW. Cationic ferritin changes outflow facility in human eyes whereas anionic ferritin does not. *Invest Ophthalmol Vis Sci*. 2001;42:1795–1802.
50. de Kater AW, Melamed S, Epstein DL. Patterns of aqueous humor outflow in glaucomatous and nonglaucomatous human eyes. A tracer study

using cationized ferritin. *Arch Ophthalmol*. 1989; 107:572–576.
51. Vranka JA, Staverosky JA, Reddy AP, et al. Biomechanical rigidity and quantitative proteomics analysis of segmental regions of the trabecular meshwork at physiologic and elevated pressures. *Invest Ophthalmol Vis Sci*. 2018;59: 246–259.
52. Kagemann L, Wang B, Wollstein G, et al. IOP elevation reduces Schlemm's canal cross-sectional area. *Invest Ophthalmol Vis Sci*. 2014;55:1805–1809.
53. Mäepea O, Bill A. The pressures in the episcleral veins, Schlemm's canal and the trabecular meshwork in monkeys: effects of changes in intraocular pressure. *Exp Eye Res*. 1989;49:645–663.
54. Mäepea O, Bill A. Pressures in the juxtacanalicular tissue and Schlemm's canal in monkeys. *Exp Eye Res*. 1992;54:879–883.
55. Buller C, Johnson D. Segmental variability of the trabecular meshwork in normal and glaucomatous eyes. *Invest Ophthalmol Vis Sci*. 1994;35: 3841–3851.
56. Swaminathan SS, Oh DJ, Kang MH, Rhee DJ. Aqueous outflow: segmental and distal flow. *J Cataract Refract Surg*. 2014;40:1263–1272.
57. McDonnell F, Dismuke WM, Overby DR, Stamer WD. Pharmacological regulation of outflow resistance distal to Schlemm's canal. *Am J Physiol Cell Physiol*. 2018;315:C44–C51.
58. Grant WM. Facility of flow through the trabecular meshwork. *AMA Arch Ophthalmol*. 1955;54: 245–248.
59. Rosenquist R, Epstein D, Melamed S, Johnson M, Grant WM. Outflow resistance of enucleated human eyes at two different perfusion pressures and different extents of trabeculotomy. *Curr Eye Res*. 1989;8:1233–1240.
60. Schuman JS, Chang W, Wang N, de Kater AW, Allingham RR. Excimer laser effects on outflow facility and outflow pathway morphology. *Invest Ophthalmol Vis Sci*. 1999;40:1676–1680.
61. Gonzalez JM, Ko MK, Hong YK, Weigert R, Tan JCH. Deep tissue analysis of distal aqueous drainage structures and contractile features. *Sci Rep*. 2017;7:17071.
62. Waxman S, Wang C, Dang Y, et al. Structure-function changes of the porcine distal outflow tract in response to nitric oxide. *Invest Ophthalmol Vis Sci*. 2018;59:4886–4895.
63. Bahler CK, Smedley GT, Zhou J, Johnson DH. Trabecular bypass stents decrease intraocular pressure in cultured human anterior segments. *Am J Ophthalmol*. 2004;138:988–994.
64. Adelman S, Shinsako D, Kiland JA, et al. The post-natal development of intraocular pressure in normal domestic cats (Felis catus) and in feline congenital glaucoma. *Exp Eye Res*. 2018;166:70–73.
65. Huang AS, Saraswathy S, Dastiridou A, et al. Aqueous angiography-mediated guidance of trabecular bypass improves angiographic outflow in human enucleated eyes. *Invest Ophthalmol Vis Sci*. 2016;57:4558–4565.
66. Huang AS, Penteado RC, Saha SK, et al. Fluorescein aqueous angiography in live normal human eyes. *J Glaucoma*. 2018;27:957–964.
67. Huang AS, Penteado RC, Papoyan V, Voskanyan L, Weinreb RN. Aqueous angiographic outflow improvement after trabecular microbypass in glaucoma patients. *Ophthalmology Glaucoma*. 2019;2:11–21.